Journal of
Composites Science

MDPI

Review

Recent Advances in Strain-Hardening UHPC with Synthetic Fibers

Jian-Guo Dai [1], Bo-Tao Huang [1] and Surendra P. Shah [2,3,*]

[1] Department of Civil and Environmental Engineering, The Hong Kong Polytechnic University, Kowloon, Hong Kong 999077, China; cejgdai@polyu.edu.hk (J.-G.D.); botaohuang@zju.edu.cn (B.-T.H.)
[2] Department of Civil Engineering, University of Texas at Arlington, Arlington, TX 76019, USA
[3] Department of Civil and Environmental Engineering, Northwestern University, Evanston, IL 60201, USA
* Correspondence: s-shah@northwestern.edu

Abstract: This paper summarizes recent advances in strain-hardening ultra-high-performance concretes (UHPC) with synthetic fibers, with emphasis on their tensile properties. The composites described here usually contain about 2.0% high-density polyethylene (PE) fibers. Compared to UHPC with steel fibers, strain-hardening UHPC with synthetic fibers generally show a higher tensile ductility, lower modulus in the cracked state, and relatively lower compressive strength. The tensile strain capacity of strain-hardening UHPC with synthetic fibers increases with increasing tensile strength. The $f'_c f_t \varepsilon_t / w$ index (compressive strength × tensile strength × tensile strain capacity/tensile crack width) is used to compare the overall performance of strain-hardening UHPC. Moreover, a probabilistic approach is applied to model the crack width distributions of strain-hardening UHPC, and estimate the critical tensile strain in practical applications, given a specific crack width limit and cumulative probability. Recent development on strain-hardening UHPC with the use of seawater, sea-sand and PE fibers are also presented.

Keywords: ultra-high-performance concrete (UHPC); strain-hardening cementitious composites (SHCC); synthetic fiber; polyethylene fiber; tensile behavior

Citation: Dai, J.-G.; Huang, B.-T.; Shah, S.P. Recent Advances in Strain-Hardening UHPC with Synthetic Fibers. *J. Compos. Sci.* **2021**, *5*, 283. https://doi.org/10.3390/jcs5100283

Academic Editor: Francesco Tornabene

Received: 4 September 2021
Accepted: 8 October 2021
Published: 18 October 2021

1. Introduction

Two major advances in recent decades in the development of cement-based materials are ultra-high-performance concrete (UHPC) and strain-hardening cementitious composites (SHCC). The emphasis on UHPC is to develop a concrete material with ultra-high compressive strength (e.g., 150–250 MPa), high tensile strength, and excellent durability [1–6]. In addition, UHPC reinforced with steel fibers can exhibit exceptional energy absorption prior to fracture and multiple cracking with extremely small crack widths prior to crack localization [2]. Compared with ordinary concrete, UHPC shows much lower water permeability and higher resistance to chloride penetration. On the other hand, the focus of SHCC is to enable fiber-reinforced cementitious composites with strain-hardening, multiple cracking, and high tensile ductility [7–13]. Naaman and Shah (1979) [7] published the first experimental test result on the strain-hardening and multiple cracking behavior of fiber-reinforced cementitious composites. Naaman (1987) [14] defined the criterion for forming multiple cracking by stating that the maximum post-cracking stress under tension must be larger than the stress at the first cracking. In addition, Shah and Shao [8,9,15,16] conducted pioneer work on discontinuous polyvinyl alcohol (PVA) fiber-reinforced SHCC fabricated by extrusion process, which exhibited a post-peak strain-hardening response with an enhanced composite strength. It was found that a larger fiber volume fraction, longer fiber length, and higher cement content lead to a higher flexural strength, a larger deflection at peak, and a higher elastic modulus [9]. Using energy considerations, Li and Leung [17,18] proposed design criteria for fiber-reinforced cementitious composites with strain-hardening and multiple cracking characteristics. Compared with conventional

concrete materials, SHCC show significantly higher ductility under both monotonic and cyclic loadings [19–21], and have been applied in new construction as well as in repair and strengthening of existing concrete structures [10,22–24].

For fiber-reinforced cementitious composites, both high matrix strength and high tensile ductility are important in practical applications. For example, UHPC with high tensile ductility can be used in the durable link slabs for jointless bridge decks or to replace steel reinforcement in 3D printing structures. The high tensile ductility of UHPC is also beneficial to its shear resistance after cracking. Therefore, strain-hardening UHPC was developed with ultra-high compressive strength, tensile strain hardening, and tensile multiple cracking. It is noted that strain-hardening UHPC can be reinforced with steel fibers or synthetic fibers. For strain-hardening UHPC with steel fibers, the compressive strength ranges from 150 to 250 MPa, and the tensile strain capacity ranges from 0.1 to 1.0% [2–4,25]. Compared with strain-hardening UHPC with steel fibers, existing strain-hardening UHPC with synthetic fibers show relatively lower compressive strength (e.g., 110–210 MPa) but higher tensile ductility (e.g., 1–10%) [11,26–30]. A strain-hardening UHPC with a compressive strength over 160 MPa and a tensile strain capacity over 3% was developed by Ranade et al., (2013) [26,27] using 2% by volume high-density polyethylene (HDPE) fibers. In 2018, Yu et al., (2018) [11] developed a PE fiber-reinforced UHPC with an ultra-high tensile ductility (8%) and a compressive strength around 120 MPa. Recently, Huang et al., (2021) [29] developed hybrid-fiber-reinforced UHPC (with 2% HDPE fibers and 1% steel fibers) that achieved an ultra-high compressive strength of 211 MPa and a high tensile ductility of 5.2%. In addition, Xu et al., (2021) [31,32] produced geopolymer aggregate ECC (using 2% HDPE fibers) with a compressive strength over 120 MPa and an ultra-high tensile ductility of 9%. It seems that the use of synthetic fibers in UHPC may become a promising way to realize the combination of ultra-high compressive strength and high tensile ductility in concrete materials.

In recent years, strain-hardening UHPC with synthetic fibers has attracted increasing attention from researchers and engineers. ACI 239 defines UHPC as concrete that has a minimum specified compressive strength of 150 MPa. In this study, the authors collected an extensive set of data from experiments carried out on high-strength strain-hardening cementitious composites reinforced with synthetic fibers. These materials used the same principles of fine particle packing and reduced porosity as UHPC but with compressive strengths ranging from 110 to 211 MPa. In the following, a summary of the recent advances of these high-strength strain-hardening cementitious composites (termed as "strain-hardening UHPC") with synthetic fibers is given while the emphasis is placed on their tensile properties. The raw materials and mix proportions of strain-hardening UHPC with synthetic fibers in existing literature are summarized, including their fiber properties and matrix materials. The overall mechanical performance (compressive, tensile, and cracking properties) of strain-hardening UHPC with synthetic fibers in existing literature are assessed and compared. In addition, the tensile properties of recently-reported strain-hardening UHPC with seawater, sea-sand, and PE fibers are also briefed. Finally, a probabilistic method is presented to model the stochastic nature and evolution of the crack width distributions of strain-hardening UHPC at different strain levels.

2. Mechanical Properties of Strain-Hardening UHPC with Synthetic Fibers

2.1. Summary of Strain-Hardening UHPC with Synthetic Fibers

The fiber properties, paste materials, and mechanical properties of strain-hardening UHPC with synthetic fibers reported in existing literature are summarized in Table 1.

Only the UHPC with a compressive strength over 120 MPa and a tensile strain capacity over 1% are presented. In addition, to assess the overall performance of strain-hardening UHPC, the compressive strength (f'_c), tensile strength (f_t), tensile strain (ε_t), and average crack width at the ultimate tensile strain (w) are listed. It is noted that the mechanical properties of strain-hardening UHPC in Table 1 are the average value of one group of samples. Among the strain-hardening UHPC in Table 1, the one developed by Huang

et al., (2021) [29] recorded the highest compressive strength (i.e., 211 MPa) and the one developed by Li et al., (2020) [32] recorded the highest tensile strain capacity (i.e., 11.0%). In the following sections, the fibers, matrices, and mechanical properties of UHPC in Table 1 will be discussed in details. It is noted that according to the suggestions in [33], some of the compressive strengths in Table 1 are corrected to the equivalent strength with the sample dimensions of 50 mm $\times$ 50 mm $\times$ 50 mm, and the corresponding values are listed in brackets.

Table 1. Summary of strain-hardening UHPC with synthetic fibers in existing literature.

Reference	Fiber Properties			Paste	Mechanical Properties				$f'_c f_t \varepsilon_t / w$ Index ($MPa^2/\mu m$)	Cross-Section of Tensile Sample (mm × mm)	Compression Sample (mm × mm × mm)
	Type and Content (Vol.)	L_f (mm)	D_f (μm)		f'_c (MPa)	f_t (MPa)	ε_t (%)	w (μm)			
Ranade et al., 2013 [26]	PE (2%)	13	28	Cem, SF, & SFl	166	14.5	3.4	180	0.45	13 × 30	50 × 50 × 50
Ranade et al., 2014 [28]	PE (2%)	13	29	Cem, SF, & SFl	205	16.1	4.6	135	1.12	13 × 30	50 × 50 × 50
Curosu et al., 2017 [34]	PE (2%)	6	20	Cem & SF	134 (139)	7.6	3.9	68 *	0.58	24 × 40	100 × 100 × 100
	Aramid (2%)	6	12		145 (151)	9.4	1.4	15 *	1.27		
	PBO-AS (2%)	6	13		140 (145)	9.8	1.4	20 *	0.96		
	PBO-HM (2%)	6	13		143 (149)	8.4	1.6	34 *	0.57		
He et al., 2017 [35]	PE (1.5%)	19	23	Cem, SF, & SFl	153	15.0	2.3	71	0.74	Not mentioned	50 × 50 × 50
Yu et al., 2018 [11]	PE (2%)	18	20	Cem, SF, & GGBS	113 (117)	17.4	8.2	160 *	1.08	13 × 30	100 × 100 × 100
Chen et al., 2018 [36]	PE (2.2%)	12	24	Cem & SF	150 (147)	10.8	2.4	48 *	0.81	13 × 30	40 × 40 × 40
Lei et al., 2019 [37]	PE (2%)	12	24	Cem, SF, & LP	163 (160)	7.0	6.5	85	0.88	13 × 30	40 × 40 × 40
Lu et al., 2019 [38]	PE (2%)	12	24	Cem & SF	132 (130)	10.4	6.4	58	1.52	13 × 30	40 × 40 × 40
Li et al., 2020 [32]	PE (2%)	18	19	Cem, SF, & FA	131	12.1	11.0	138	1.26	13 × 30	50 × 50 × 50
Liu et al., 2021 [39]	PE (1.5%)	18	20	Cem, FA, & SF	129	13.5	9.7	288	0.59	13 × 30	Not mentioned
Huang et al., 2021 [29]	PE (2%) +ST (1%)	PE: 12 ST: 13	PE: 24 ST: 200	Cem, GGBS, SF, & QP	211	16.1	5.2	72	2.45	13 × 30	50 × 50 × 50

Note: * represents that this value was estimated based on the data in the corresponding reference. The mechanical properties are the average value of one group of samples. All mixtures used superplasticizers in various quantities. PE = high-density polyethylene fiber, Aramid = poly(p-phenylene-terephthalamide) (aramid) fiber, PBO-AS = as-spun poly (p-phenylene-2,6-benzobisoxazole) (PBO) fiber, PBO-HM = high-modulus PBO fiber, and ST = steel fiber; Paste materials: Cem = cement, SF = silica fume, SFl = silica flour, LP = limestone powder, GGBS = ground granulated blast furnace slag, QP = quartz powder, and FA = fly ash; Mechanical properties: f'_c = compressive strength, f_t = tensile strength, ε_t = tensile strain, and w = average crack width at the ultimate tensile strain.

2.2. Fiber

Among the existing strain-hardening UHPC with synthetic fibers, four types of synthetic fibers were used (Table 1), including high-density polyethylene (PE) fibers, poly (p-phenylene-terephthalamide) (aramid) fibers, as-spun poly (p-phenylene-2,6-benzobisoxazole) (PBO-AS) fibers, and high-modulus PBO (PBO-HM) fibers. In addition, steel fibers were also used to reinforce the strain-hardening UHPC together with PE fibers in a hybrid manner [29]. The properties of these used fibers are summarized in Table 2. In the table the properties of PVA fibers are also presented for comparison, which are widely used in normal-strength strain-hardening cementitious composites. For the strain-hardening UHPC in Table 2, the fiber volumetric content used varied between 1.5% and 3.0%. PE fibers with 2% volume fraction were most commonly used, and the fiber length and diameter were 6–19 mm and 12–29 μm, respectively. Compared with PVA fibers in normal-strength strain-hardening cementitious composites, PE fibers have higher modulus and tensile strength, which are needed to achieve strain-hardening behavior in a high-strength matrix.

Table 2. Fiber properties.

Fiber Type	Length (mm)	Diameter (μm)	Density g/cm ^{3}	Young's Modulus (GPa)	Tensile Strength (GPa)	Elongation (%)
PVA	8–12	24–39	1.3	25–40	0.8–1.6	6.0
PE	6–19	12–29	0.97	80–120	2.5–3.8	3.1–8.0
PBO-AS	6	13	1.54	180	5.8	3.5
PBO-HM	6	13	1.56	270	5.8	2.5
Aramid	6	12	1.39	74	3.4	4.5
Steel	13	200	7.8	210	2.0	5.0

Note: The properties of PVA fiber were obtained from the manufacturer Kuraray and Nycon. The properties of PE, PBO-AS, PBO-HM, Aramid, and steel fibers were obtained from the corresponding literature of strain-hardening UHPC in Table 1.

Curosu et al., (2017) [34] used aramid, PBO-AS and PBO-HM fibers to develop strain-hardening UHPC. Compared to the strain-hardening UHPC with PE fibers, the UHPC made with the aramid and PBO fibers showed a higher cracking strength and a smaller crack width, and the UHPC with aramid and PBO-AS fibers also showed a higher tensile strength and more pronounced multiple cracking. In addition, the fiber-matrix bond of aramid and PBO fibers was reported to be higher than that of PE fibers, owing to the lower hydrophobic characteristic of the formers compared with the latter. Huang et al., (2021) [29] developed strain-hardening UHPC with a compressive strength of 211 MPa and a tensile strain capacity of 5.2% based on the use of hybrid fiber reinforcement (2% PE fibers and 1% steel fibers), and they observed partial PE fiber rupture at the ultimate state, suggesting an efficient use of high-strength synthetic fibers in strain-hardening UHPC.

2.3. Matrix

The raw materials of strain-hardening UHPC paste are listed in Table 1. Cement (Cem) and silica fume (SF) were consistently used in all the UHPC, and the silica fume-to-cement ratio was 0.20–0.30, which is also widely used in other UHPC materials. In addition, silica flour (SFl), limestone powder (LP), quartz powder (QP), and fly ash (FA) were also used in some of the paste. The water-to-cementitious binder ratio was commonly 0.15–0.20. Generally speaking, the paste materials of strain-hardening UHPC with synthetic fibers are similar to other UHPC materials, but the matrix shows a comparatively low sand-to-binder ratio. Heat curing (90 °C) was used for some of the strain-hardening UHPC to enhance the matrix strength.

According to the literature presented, all the UHPC with 2% PE fiber content were prepared in laboratory. The commonly-used mixing process using small-volume mixer was as follows: (1) the raw materials of the matrix were dry mixed for 2–3 min; (2) the water and super-plasticizers were added and mixed for 5–10 min; and (3) the fibers were then added and mixed for another 5–10 min. It seems that the mixing of UHPC with 2% PE

fibers by large-volume mixer remains challenging, and more efforts are needed on this important issue in future study.

2.4. Tensile Performance

Figure 1a shows a typical tensile stress - strain curve of strain-hardening UHPC with 2% PE fibers at the age of 28 days [11]. It is clear that the specimen exhibited tensile strain-hardening behavior. The DIC images of the tensile specimen at different strain levels are also presented in Figure 1a. It is clear that multiple cracks saturated over the interested area as the strain level increases. Most importantly, cracks were not localized even under a high tensile strain level. The microstructure and morphology of the strain-hardening UHPC sample were observed on fractured surfaces using secondary electron imaging (Figure 1b). Due to the high strength of the matrix and the large aspect ratio (i.e., L_f/d_f = 900) of PE fiber, the bond strength between the PE fiber and the matrix was strong enough to fracture the PE fiber. Several fracture surfaces of PE fibers were observed.

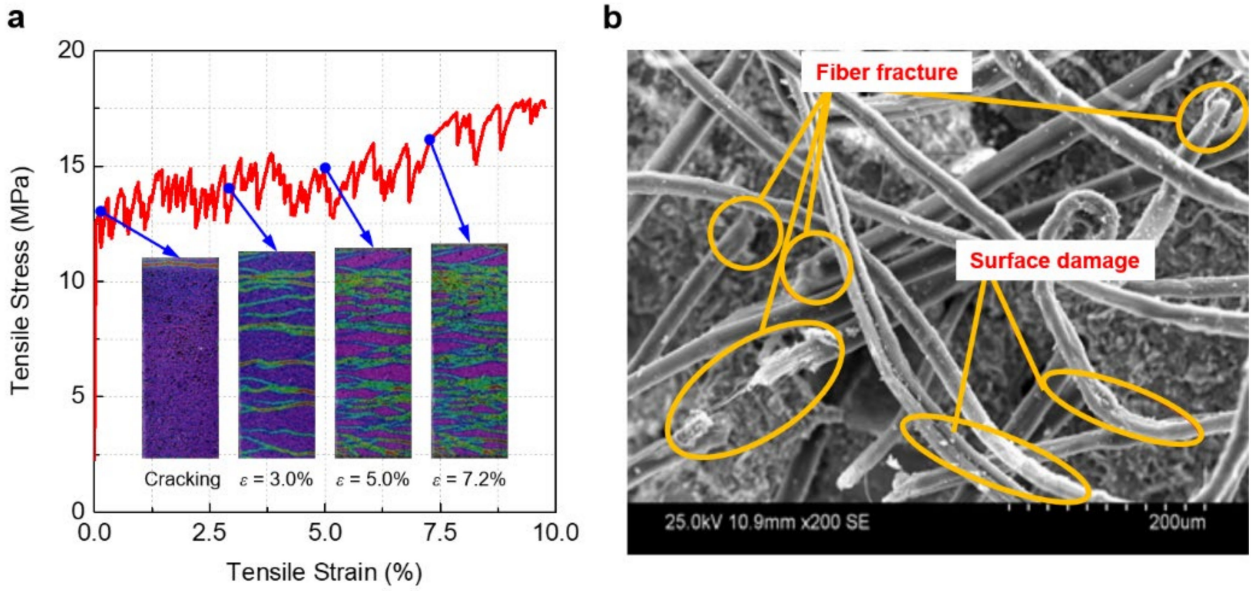

Figure 1. Strain-hardening UHPC with PE fibers developed by Yu et al., (2018): (**a**) tensile stress–strain relation and cracking mode; and (**b**) SEM image of PE fibers on tensile failure surface. (Reproduced with permission from [11]).

The tensile stress–strain relations of the hybrid-fiber-reinforced strain-hardening UHPC with a compressive strength of 211 MPa are presented in Figure 2. The UHPC achieved an average tensile strength of 16 MPa and an average strain capacity of 5.2%. The average crack width at the ultimate tensile strain was found to be 72 μm, due to the use of high fiber volume (3%), and more importantly, a hybrid use of steel fibers (1%) and PE fibers (2%). Consequently, the crack widths under the service condition would be much smaller, which is beneficial to the durability performance of strain-hardening UHPC under combined mechanical and environmental loadings. Figure 2 also presents the DIC strain fields and crack patterns at four strain levels, and significant multiple cracking phenomena can be observed.

It should be pointed out that the mechanism of the tensile behavior of strain-hardening UHPC with synthetic fibers were similar, which follows both the strength and energy criteria proposed by Li and Leung [17]. For the strength criterion, the maximum fiber-bridging stress must be no less than the first-cracking stress of the matrix. For the energy criterion, the complementary energy J_b' of the fiber-bridging stress vs. crack opening relation must be no less than the crack tip toughness of matrix J_{tip}. Based on these two criteria, steady-state and multiple cracking of the mixtures in Table 1 can be achieved.

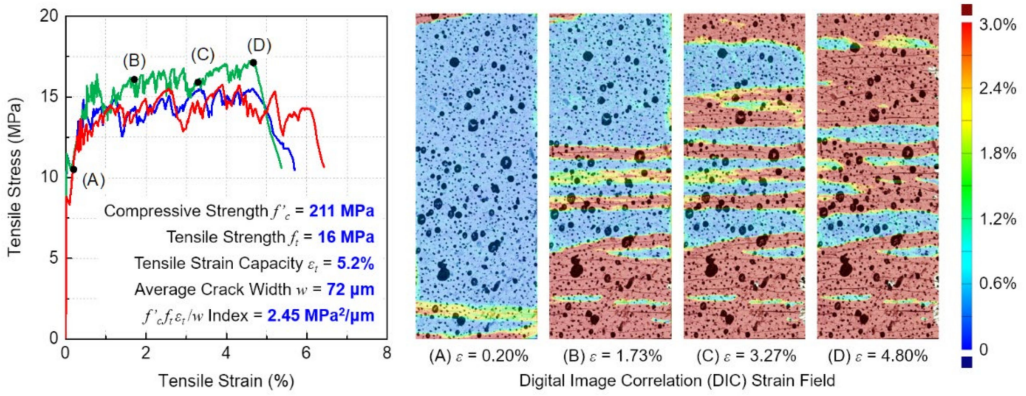

Figure 2. Tensile stress–strain relation and DIC strain field of strain-hardening UHPC with a combination of PE fibers and steel fibers developed by Huang et al., (2021). (Reproduced with permission from [29]).

Figure 3 presents the tensile strain capacity vs. the tensile strength relation based on the data from Table 1 and Yu et al., (2020) [40]. It should be pointed out that the strain-hardening UHPC with PE fibers reported in [40] used a constant matrix but variable fiber aspect ratios and contents. A trend line of all the data points is plotted in Figure 3 based on linear fitting. It is clearly seen that the higher the tensile strength, the higher the tensile strain capacity. It should be noted that in Figure 3, the tensile ductility exhibits large scatter given the same tensile strength, because the latter is more dominated by the tensile capacity of fibers while the former is influenced by many other factors such as the fiber-matrix bond and the matrix toughness.

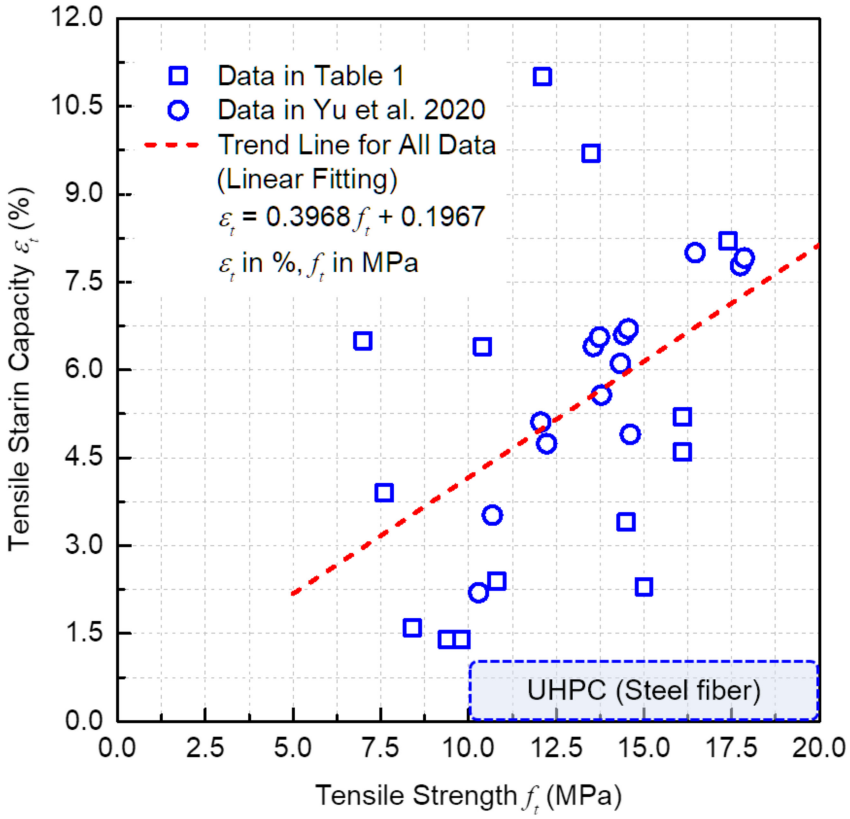

Figure 3. Tensile strain capacity vs. tensile strength data from Table 1 and reference [40].

It should be pointed out that the small specimens used in Table 1 could have led to overestimated tensile performance, because different sizes of tensile specimens can have

noticeable difference in terms of tensile strength and ductility [41]. The small thickness of the tensile samples (13 mm) will influence the fiber orientation significantly. For such specimens, the 18-mm PE fiber in Table 1 should be considered as a two-dimensional distribution rather than a three-dimensional distribution. Hence, the measured tensile ductility and strength were overestimated. In future study, more attention needs be to paid to the tensile behavior of PE fiber-reinforced UHPC with three-dimensional fiber distribution.

3. Overall Assessment of Mechanical Properties of Strain-Hardening UHPC

Figure 4 presents compressive strength vs. tensile strain capacity relations of the strain-hardening UHPC in Table 1. For comparison, the strength vs. ductility relation of strain-hardening UHPC with the sole use of steel fibers is also presented in Figure 4. Generally, the compressive strength of strain-hardening UHPC with steel fibers is 150–250 MPa, and the tensile strain capacity is below 1.0%, while the compressive strength of strain-hardening UHPC with synthetic fibers was 122–211 MPa, and the rupture strain was 1.4–11.0%. It is noted that more than half of the strain-hardening UHPC with synthetic fibers showed a compressive strength below 150 MPa. Compared to UHPC with steel fibers, UHPC with synthetic fibers exhibited higher tensile ductility but comparatively low compressive strength.

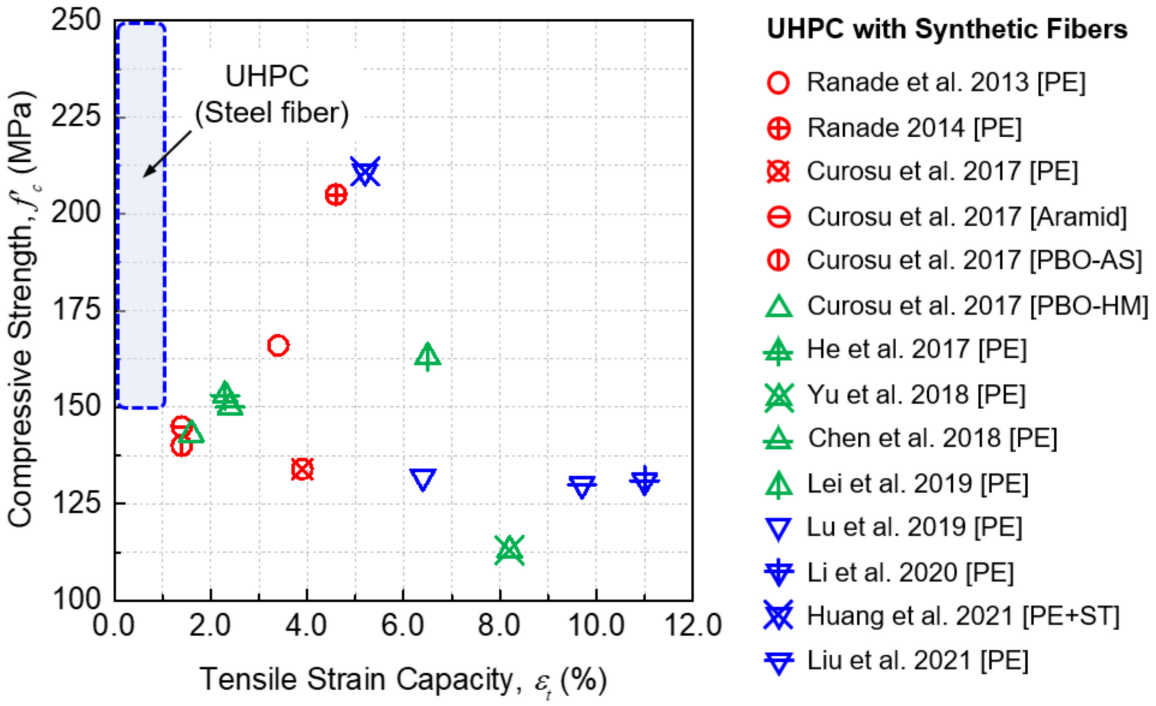

Figure 4. Compressive strength vs. tensile strain capacity relations of strain-hardening UHPC with synthetic fibers in existing literature.

For strain-hardening UHPC, compressive strength (f'_c), tensile ductility (ε_t), tensile strength (f_t), and average crack width (w) at the ultimate tensile strain are all important for practical applications. Table 1 summarizes the aforementioned mechanical properties. It should be noted that some of the crack widths were estimated based on the data in the corresponding reference, as the actual values were not reported. To assess the overall performance of strain-hardening UHPC, an index of $f'_c f_t \varepsilon_t / w$ (compressive strength (unit: MPa) × tensile strength (unit: MPa) × tensile strain capacity (unit: 1)/tensile crack width (unit: μm)) was introduced by Huang et al., (2021) [29]. As a smaller crack width (w) is beneficial to the durability of UHPC, the reciprocal of w is used. Note that for the $f'_c f_t \varepsilon_t / w$ index, the larger the value, the better the performance.

Figure 5 presents a summary of $f'_c f_t \varepsilon_t / w$ indices of all strain-hardening UHPC in Table 1. The strain-hardening UHPC developed by Huang et al., (2021) [29] recorded the highest $f'_c f_t \varepsilon_t / w$ index (i.e., 2.45 MPa^2/μm), which was reinforced by 2% (vol.) PE fiber and 1% (vol.) steel fiber. Lu et al., (2019) [38] used graphene oxide to strengthen the bond between the PE fiber and the matrix to improve the strain-hardening behavior, and the corresponding $f'_c f_t \varepsilon_t / w$ index was 1.52 MPa^2/μm. The third highest $f'_c f_t \varepsilon_t / w$ index was achieved by strain-hardening UHPC with aramid fibers. It is expected that the $f'_c f_t \varepsilon_t / w$ index can also be applied to assess the overall performance of UHPC with steel fibers. In Figure 5, as a reference the result of UHPC with steel fibers from Wille et al., (2014) [2] is also presented with the following properties f'_c = 250 MPa, f_t = 20 MPa, ε_t = 0.6%, and w = 40 μm.

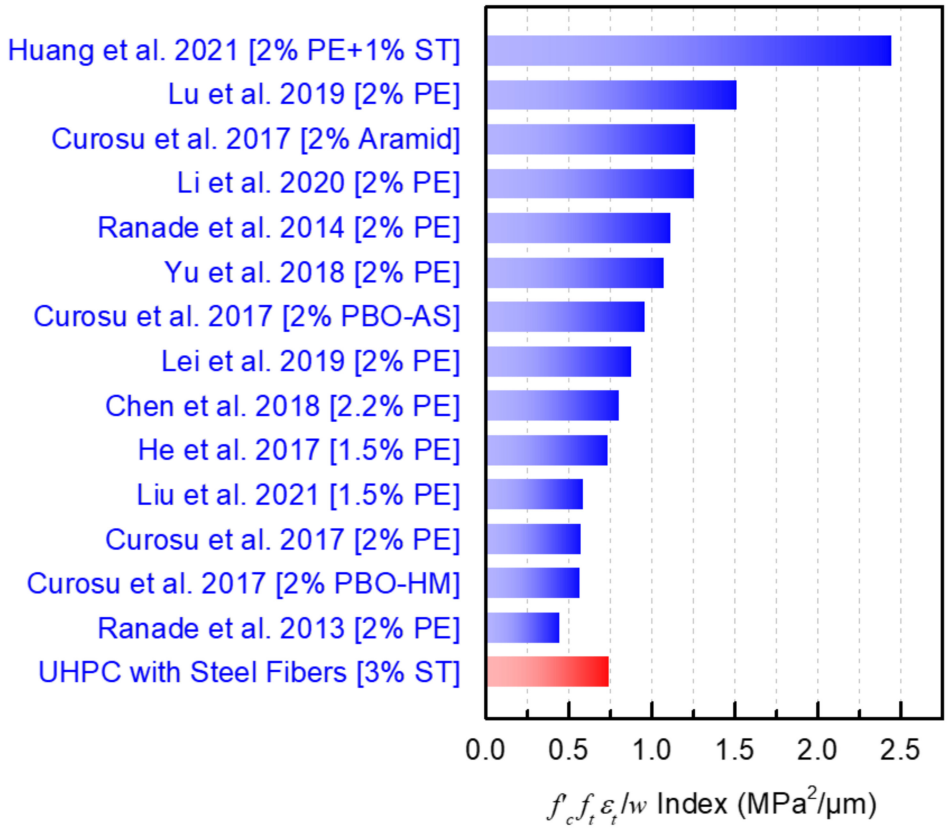

Figure 5. Summary of $f'_c f_t \varepsilon_t / w$ indices of strain-hardening UHPC with synthetic fibers.

4. Use of Seawater and Sea-Sand with UHPC and PE Fibers

Recently, the seawater sea-sand UHPC was explored for marine and coastal concrete structures with non-corrosive reinforcements (e.g., fiber-reinforced polymer (FRP), stainless steel, and steel-FRP composite reinforcements) [42–44]. It is worth noting that seawater and sea-sand may not be suitable for producing UHPC with steel fibers, as steel fibers may be corroded. In such cases, synthetic fibers (e.g., PE fibers) are preferable for the production of strain hardening seawater sea-sand UHPC (SS-UHPC) [45–47]. Table 3 presents several mix proportions of SS-UHPC with PE fibers (different fiber lengths and content), and Figure 6 summarizes their compressive and tensile properties, where the effects of seawater, sea-sand, fiber length, and fiber content are presented.

Table 3. Material IDs of SS-UHPC with PE fibers in this study.

Specimen Code	Fiber Length (mm)	Fiber Content (%)	Water	Sand
Control	12	2.0	Freshwater	Washed sea-sand
PE12mm-1.0%	12	1.0	Seawater	Unwashed sea-sand
PE12mm-1.5%	12	1.5		
PE12mm-2.0%	12	2.0		
PE06mm-2.0%	6	2.0		
PE18mm-2.0%	12	2.0		

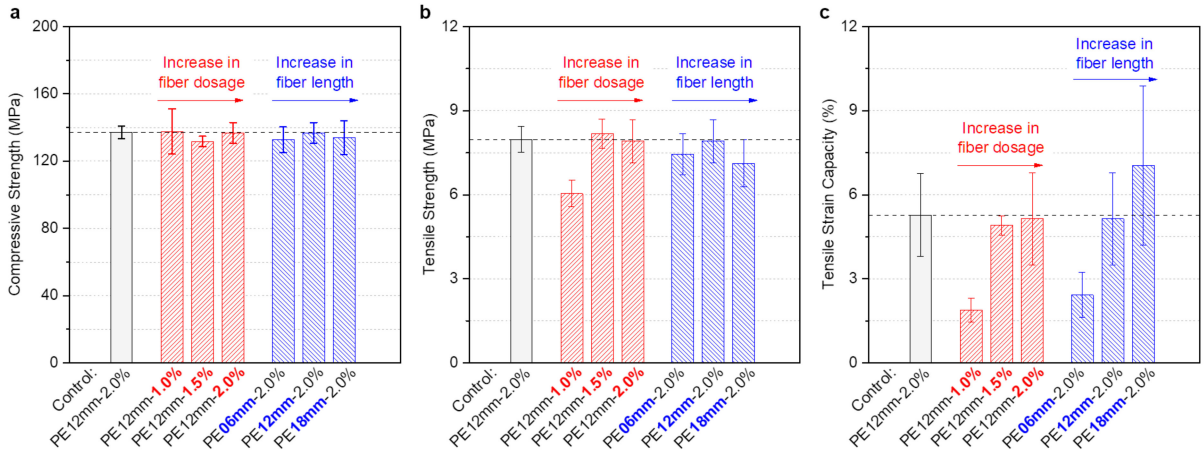

Figure 6. Mechanical properties of SS-UHPC: (**a**) compressive strength; (**b**) tensile strength; and (**c**) tensile strain capacity [46].

The compressive strength of PE12mm-2.0% was 136.8 MPa, while the strength of control SS-UHPC was 137.1 MPa. The effect of fiber content (1% to 2%) and length (6 mm to 18 mm) on the compressive strength of SS-UHPC was marginal. For tensile properties, no obvious differences were observed in the 28-day tensile strength and ductility between PE12mm-2.0% and the control group. As the fiber content increased from 1.0% to 2.0%, the tensile ductility and strength increased. The tensile strain capacity and strength of PE12mm-1.5% and PE12mm-2.0% were close to each other, and hence the fiber content of 1.5% seems to be enough to achieve both high tensile ductility and strength in SS-UHPC. As the fiber length increased, the strain capacity increased while the tensile strength changed little. The setting time of SS-UHPC was found to be slightly shorter than that of freshwater washed-sand UHPC. However, using seawater and sea-sand seemed to not change significantly the fiber-matrix bond as well as the tensile strength and ductility of SS-UHPC [46].

It is noted that the long-term mechanical performance and durability of seawater sea-sand UHPC are critical for this emerging material, and future research is suggested to explore these issues. In addition, as the PE fibers were used in seawater sea-sand UHPC, the high-temperature performance of this material may not be good, because the melting point of PE fiber (170 °C) is comparatively low. To address this issue, PBO fibers (melting point: 650 °C) could be used to improve the high-temperature performance.

5. Probabilistic Modeling of Crack Width Distribution of Strain-Hardening UHPC

The crack widths of strain-hardening UHPC at different strain levels are important for practical applications. In this section, a probabilistic model is presented to describe the crack width evolution of strain-hardening UHPC with PE fibers, which was proposed by Huang et al., (2021) [47]. Figure 7 presents the crack pattern of a strain-hardening UHPC sample. The strain level A is set as 0.20%; the strain level E is the tensile strain capacity; and the strain levels B, C, and D divide the strain range between A and E into quarters. The

crack widths were obtained from high-resolution digital photos, which are summarized in Table 4. It is noted that the above result is a representative case selected from [47], and the full database can also be found in [47].

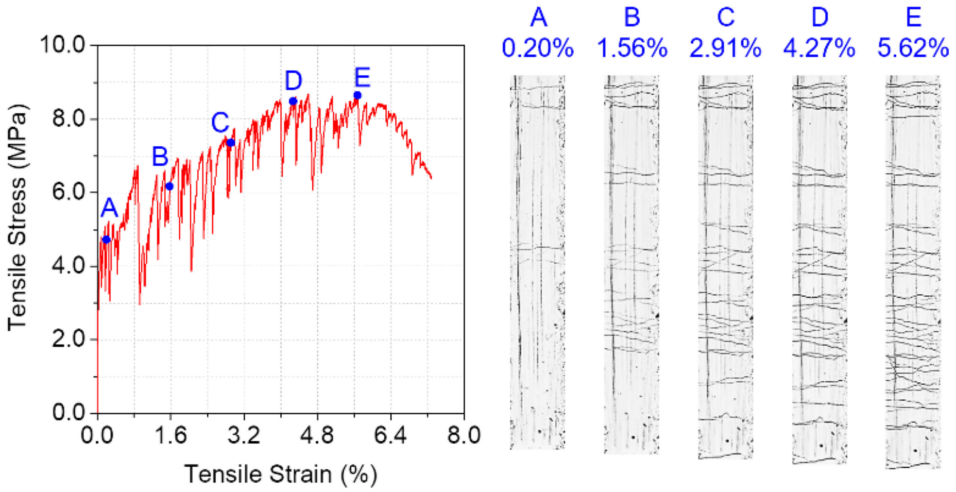

Figure 7. Crack patterns of strain-hardening UHPC with PE fibers. (Reproduced with permission from [47]).

Table 4. Crack widths and distributions of strain-hardening UHPC with PE fibers. (Reproduced with permission from [47]).

Strain (%)	Number of Cracks									Weibull Distribution		
	0–15 µm	15–30 µm	30–45 µm	45–60 µm	60–75 µm	75–90 µm	90–105 µm	105–120 µm	>120 µm	λ	k	r
A: 0.20	1	2	2	0	0	0	0	0	0	39.1	2.09	0.94
B: 1.56	3	7	8	7	0	0	0	0	0	47.9	2.55	0.96
C: 2.92	4	7	9	9	4	2	0	0	0	55.8	2.31	0.98
D: 4.28	2	7	11	8	7	4	1	0	0	62.6	2.42	0.98
E: 5.64	2	10	8	15	7	3	0	2	1 (150 µm)	63.7	2.49	0.98

The probabilistic model for the crack width evolution of strain-hardening UHPC can be obtained as follows. First, the cumulative distributions of crack widths at different strain levels were found to follow the Weibull function (Equation (1)), as the correlation coefficient r in Table 4 is close to 1. It is noted that the correlation coefficient in this section was obtained from the curve fitting using Origin 9.1 software.

$$F_W(w_0) = 1 - \exp\left(-\left(\frac{w_0}{\lambda}\right)^k\right) \quad (1)$$

where w_0 is the crack width; λ and k are the scale and shape parameters of the Weibull function, respectively; and $F_w(w_0)$ is the cumulative distribution function.

Second, the functions linking λ and k to the tensile strain levels are introduced. It was found that λ increased almost linearly with increasing tensile strain ε. Therefore, Equation (2) can be obtained:

$$\lambda = A\varepsilon + B \quad (2)$$

where A and B are the coefficients from the linear fitting. Equation (2) indicates that the average crack width increases linearly with the tensile strain. For the sample in Figure 7, A = 4.7 and B = 40.1 µm, and the correlation coefficient r is 0.974 (close to 1). As the variation of the k values at different strain levels is limited, for simplicity, the Weibull shape parameter k is assumed to be a constant (using the average value k_{avg}) (Equation (3)). For the sample in Figure 7, k_{avg} = 2.37.

$$k = k_{avg} \quad (3)$$

Third, by introducing Equation (2) and Equation (3) into Equation (1), the cumulative distribution of w_0 at a given tensile strain ε can be expressed as:

$$F(w_0) = 1 - \exp\left(-\left(\frac{w_0}{A\varepsilon + B}\right)^{k_{avg}}\right) \quad (4)$$

According to Equation (4), the following equation can be obtained.

$$w_0 = (A\varepsilon + B)(-\ln(1 - F(w_0)))^{1/k_{avg}} \quad (5)$$

In Equation (5), for a given tensile strain ε and cumulative probability $F(w_0)$, the crack width w_0 can be calculated.

The model and test results of the crack width distributions at different strain levels are plotted in Figure 8. The crack width vs. tensile strain relation at three cumulative probabilities (0%, 50% and 99%) are also presented. The model results show good agreement with the test ones, indicating that the model can describe the crack width evolution of strain-hardening UHPC. To control the crack width in practical applications, the model can be used to estimate the critical tensile strain of UHPC for a given crack width limit and cumulative probability. For instance, by setting $F(w_0)$ = 99% and $w_{99\%}$ = 100 μm in Equation (5), the critical tensile strain of the sample in Figure 8 should be no more than 2.64%. It is expected that this model can also be used for strain-hardening UHPC with steel fibers. In future studies, this method can also be applied to model the crack width evolution of other strain-hardening cement-based materials [31,48,49].

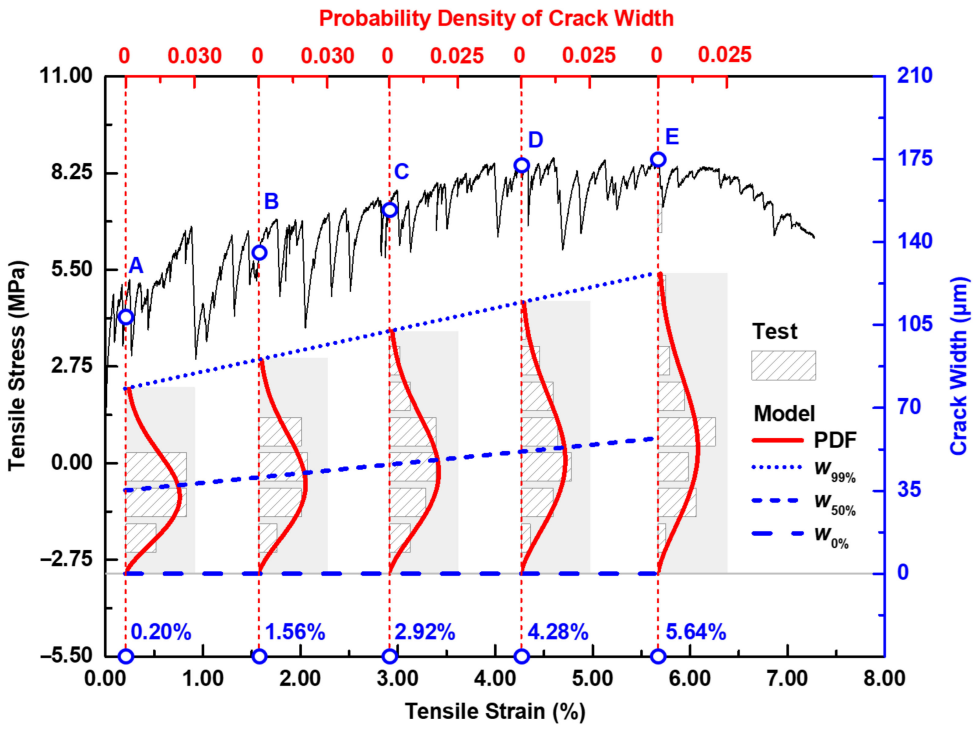

Figure 8. Model and test results of crack width distributions of strain-hardening UHPC with PE fibers at different tensile strain levels. (Reproduced with permission from [47]).

6. Conclusions

In this study, recent advances of strain-hardening UHPC with synthetic fibers are summarized, including their mechanical properties (especially tensile properties), raw materials used (fiber, matrix, and utilization of seawater and sea-sand), and probabilistic modeling of crack width evolution. The following conclusions can be drawn.

- Among the strain-hardening UHPC with synthetic fibers, PE fibers with 2% volume fraction were most commonly used, and the fiber length and diameter were 6–19 mm and 12–29 μm, respectively. The paste raw materials of strain-hardening UHPC with synthetic fibers are similar to other UHPC, but with a comparatively low sand-to-binder ratio (commonly 0.2–0.5).
- The tensile strain capacity of strain-hardening UHPC with synthetic fibers increases with its tensile strength.
- For the same fiber volume fraction, strain-hardening UHPC with synthetic fibers show higher tensile ductility but lower compressive strength than strain-hardening UHPC with steel fibers. The index $f'_c f_t \varepsilon_t / w$ can be used to compare their overall performance. To the best of the authors knowledge, the use of seawater and sea-sand in UHPC (SS-UHPC) with PE fibers appears to be a new development. SS-UHPC with a compressive strength over 130 MPa, a tensile strength over 8 MPa and a tensile strain capacity over 5% is described. Overall, it is observed that using seawater and sea-sand had almost no negative effects on the 28-day mechanical properties of strain-hardening UHPC with PE fibers.
- The probabilistic approach followed here can be used to model the stochastic nature and evolution of the crack width distributions of strain-hardening UHPC at different strain levels; it can be applied to estimate the critical tensile strain of strain-hardening UHPC for a specific crack width limit and cumulative probability.

Author Contributions: Conceptualization, J.-G.D. and S.P.S.; methodology, B.-T.H.; validation, B.-T.H.; formal analysis, B.-T.H.; writing—original draft preparation, B.-T.H.; writing—review and editing, J.-G.D. and S.P.S.; visualization, B.-T.H.; supervision, J.-G.D. and S.P.S.; project administration, J.-G.D.; funding acquisition, J.-G.D. All authors have read and agreed to the published version of the manuscript.

Funding: This study was supported by the Hong Kong Research Grants Council—Theme-based Research Scheme (Project No.: T22-502/18-R), the Research Institute for Sustainable Urban Development, The Hong Kong Polytechnic University (Project No. 1-BBWE), and the Hong Kong Innovation and Technology Fund through the Research Talent Hub (Project No. ITS/077/18FX).

Institutional Review Board Statement: Not applicable.

Informed Consent Statement: Not applicable.

Data Availability Statement: The data presented in this study are available on request.

Acknowledgments: The authors would like to thank Antoine E. Naaman for providing a helpful review.

Conflicts of Interest: The authors declare no conflict of interest.

References

1. Richard, P.; Cheyrezy, M. Composition of reactive powder concretes. *Cem. Concr. Res.* **1995**, *25*, 1501–1511. [CrossRef]
2. Wille, K.; El-Tawil, S.; Naaman, A. Properties of strain hardening ultra high performance fiber reinforced concrete (UHP-FRC) under direct tensile loading. *Cem. Concr. Compos.* **2014**, *48*, 53–66. [CrossRef]
3. Wille, K.; Naaman, A.E.; El-Tawil, S. Optimizing ultra-high performance fiber-reinforced concrete. *Concr. Int.* **2011**, *33*, 35–41.
4. Wille, K.; Kim, D.J.; Naaman, A.E. Strain-hardening UHP-FRC with low fiber contents. *Mater. Struct.* **2011**, *44*, 583–598. [CrossRef]
5. Wille, K.; Naaman, A.E.; Parra-Montesinos, G.J. Ultra-high performance concrete with compressive strength exceeding 150 MPa (22 ksi): A Simpler Way. *ACI Mater. J.* **2011**, *108*, 34–46.
6. Huang, B.T.; Dai, J.G.; Weng, K.F.; Zhu, J.X.; Shah, S.P. Flexural performance of UHPC-concrete-ECC composite member reinforced by perforated steel plate. *J. Struct. Eng.* **2021**, *147*, 04021065. [CrossRef]
7. Naaman, A.; Shah, S. Fracture and Multiple Cracking of Cementitious Composites. In *Fracture Mechanics Applied to Brittle Materials*; ASTM International: West Conshohocken, PA, USA, 1979; pp. 183–201.
8. Shah, S.P.; Shao, Y. Extrusion processing of fiber-reinforced cement-matrix composites. In Proceedings of the 1994 International Mechanical Engineering Congress and Exposition, Chicago, IL, USA, 6–11 November 1994; pp. 205–210.
9. Shao, Y.; Shah, S.P. Mechanical properties of PVA fiber reinforced cement composites fabricated by extrusion pro-cessing. *ACI Mater. J.* **1997**, *94*, 555–564.

10. Li, V.C. *Engineered Cementitious Composites (ECC)-Bendable Concrete for Sustainable and Resilient Infrastructure*; Springer Verlag GmbH: Berlin/Heidelberg, Germany, 2019.
11. Yu, K.; Yu, J.-T.; Dai, J.-G.; Lu, Z.-D.; Shah, S.P. Development of ultra-high performance engineered cementitious composites using polyethylene (PE) fibers. *Constr. Build. Mater.* **2018**, *158*, 217–227. [CrossRef]
12. Huang, B.T.; Li, Q.H.; Xu, S.L.; Zhou, B.M. Tensile fatigue behavior of fiber-reinforced cementitious material with high ductility: Experimental study and novel PSN model. *Constr. Build. Mater.* **2018**, *178*, 349–359. [CrossRef]
13. Huang, B.T.; Li, Q.H.; Xu, S.L.; Zhang, L. Static and fatigue performance of reinforced concrete beam strengthened with strain-hardening fiber-reinforced cementitious composite. *Eng. Struct.* **2019**, *199*, 109576. [CrossRef]
14. Naaman, A.E. High performance fiber reinforced cement composites. In Proceedings of the IABSE Symposium on Concrete Structures for the Future, Zurich, Switzerland, 7–11 September 1987; pp. 371–376. [CrossRef]
15. Shao, Y.; Marikunte, S.; Shah, S.P. Extruded fiber-reinforced composites. *Concr. Int.* **1995**, *17*, 48–53.
16. Shao, Y.; Qiu, J.; Shah, S.P. Microstructure of extruded cement-bonded fiberboard. *Cem. Concr. Res.* **2001**, *31*, 1153–1161. [CrossRef]
17. Li, V.; Leung, C.K.Y. Steady-state and multiple cracking of short random fiber composites. *J. Eng. Mech.* **1992**, *118*, 2246–2264. [CrossRef]
18. Leung, C.K.Y. Design criteria for pseudoductile fiber-reinforced composites. *J. Eng. Mech.* **1996**, *122*, 10–18. [CrossRef]
19. Zhou, J.; Pan, J.; Leung, C.K.Y. Mechanical behavior of fiber-reinforced engineered cementitious composites in uniaxial compression. *J. Mater. Civ. Eng.* **2015**, *27*, 04014111. [CrossRef]
20. Huang, B.T.; Li, Q.H.; Xu, S.L.; Liu, W.; Wang, H.T. Fatigue deformation behavior and fiber failure mechanism of ultra-high toughness cementitious composites in compression. *Mater. Des.* **2018**, *157*, 457–468. [CrossRef]
21. Huang, B.-T.; Li, Q.-H.; Xu, S.-L. Fatigue deformation model of plain and fiber-reinforced concrete based on Weibull function. *J. Struct. Eng.* **2019**, *145*, 04018234. [CrossRef]
22. Rokugo, K.; Kanda, T.; Yokota, H.; Sakata, N. Applications and recommendations of high performance fiber rein-forced cement composites with multiple fine cracking (HPFRCC) in Japan. *Mater. Struct.* **2009**, *42*, 1197. [CrossRef]
23. Huang, B.T.; Li, Q.H.; Xu, S.L.; Li, C.F. Development of reinforced ultra-high toughness cementitious composite permanent formwork: Experimental study and Digital Image Correlation analysis. *Compos. Struct.* **2017**, *180*, 892–903. [CrossRef]
24. Huang, B.T.; Li, Q.H.; Xu, S.L.; Zhou, B. Strengthening of reinforced concrete structure using sprayable fiber-reinforced cementitious composites with high ductility. *Compos. Struct.* **2019**, *220*, 940–952. [CrossRef]
25. Wille, K.; Naaman, A.E.; El-Tawil, S.; Parra-Montesinos, G.J. Ultra-high performance concrete and fiber reinforced concrete: Achieving strength and ductility without heat curing. *Mater. Struct.* **2011**, *45*, 309–324. [CrossRef]
26. Ranade, R.; Li, V.C.; Stults, M.D.; Heard, W.F.; Rushing, T.S. Composite properties of high-strength, high-ductility concrete. *ACI Mater. J.* **2013**, *110*, 413–422.
27. Ranade, R.; Li, V.C.; Stults, M.D.; Rushing, T.S.; Roth, J.; Heard, W.F. Micromechanics of high-strength, high-ductility concrete. *ACI Mater. J.* **2013**, *110*, 375.
28. Ranade, R. Advanced Cementitious Composite Development for Resilient and Sustainable Infrastructure. Ph.D. Thesis, University of Michigan, Ann Arbor, MI, USA, 2014.
29. Huang, B.T.; Weng, K.F.; Zhu, J.X.; Xiang, Y.; Dai, J.G.; Li, V.C. Engineered/strain-hardening cementitious composites (ECC/SHCC) with an ultra-high compressive strength over 210 MPa. *Compos. Commun.* **2021**, *26*, 100775. [CrossRef]
30. Li, Y.; Guan, X.; Zhang, C.; Liu, T. Development of high-strength and high-ductility ECC with saturated multiple cracking based on the flaw effect of coarse river sand. *J. Mater. Civ. Eng.* **2020**, *32*, 04020317. [CrossRef]
31. Xu, L.Y.; Huang, B.T.; Dai, J.G. Development of engineered cementitious composites (ECC) using artificial fine aggregates. *Constr. Build. Mater.* **2021**, *305*, 124742. [CrossRef]
32. Xu, L.Y.; Qian, L.P.; Huang, B.T.; Dai, J.G. Development of artificial one-part geopolymer lightweight aggregates by crushing technique. *J. Clean. Prod.* **2021**, *315*, 128200. [CrossRef]
33. Yu, K.; Ding, Y.; Zhang, Y. Size effects on tensile properties and compressive strength of engineered cementitious composites. *Cem. Concr. Compos.* **2020**, *113*, 103691. [CrossRef]
34. Curosu, I.; Liebscher, M.; Mechtcherine, V.; Bellmann, C.; Michel, S. Tensile behavior of high-strength strain-hardening cement-based composites (HS-SHCC) made with high-performance polyethylene, aramid and PBO fibers. *Cem. Concr. Res.* **2017**, *98*, 71–81. [CrossRef]
35. He, S.; Qiu, J.; Li, J.; Yang, E.-H. Strain hardening ultra-high performance concrete (SHUHPC) incorporating CNF-coated polyethylene fibers. *Cem. Concr. Res.* **2017**, *98*, 50–60. [CrossRef]
36. Chen, Y.; Yu, J.; Leung, C.K. Use of high strength Strain-hardening cementitious composites for flexural repair of concrete structures with significant steel corrosion. *Constr. Build. Mater.* **2018**, *167*, 325–337. [CrossRef]
37. Lei, D.Y.; Guo, L.P.; Chen, B.; Curosu, I.; Mechtcherine, V. The connection between microscopic and macroscopic properties of ultra-high strength and ultra-high ductility cementitious composites (UHS-UHDCC). *Compos. Part B Eng.* **2019**, *164*, 144–157. [CrossRef]
38. Lu, Z.; Yao, J.; Leung, C.K. Using graphene oxide to strengthen the bond between PE fiber and matrix to improve the strain hardening behavior of SHCC. *Cem. Concr. Res.* **2019**, *126*, 105899. [CrossRef]
39. Liu, T.; Bai, R.; Chen, Z.; Li, Y.; Yang, Y. Tailoring of polyethylene fiber surface by coating silane coupling agent for strain hardening cementitious composite. *Constr. Build. Mater.* **2021**, *278*, 122263. [CrossRef]

40. Yu, K.Q.; Lu, Z.D.; Dai, J.G.; Shah, S.P. Direct tensile properties and stress–strain model of UHP-ECC. *J. Mater. Civ. Eng.* **2020**, *32*, 04019334. [CrossRef]
41. Aghdasi, P.; Heid, A.E.; Chao, S.-H. Developing ultra-high-performance fiber-reinforced concrete for large-scale structural applications. *ACI Mater. J.* **2016**, *113*, 559–570. [CrossRef]
42. Teng, J.G.; Xiang, Y.; Yu, T.; Fang, Z. Development and mechanical behaviour of ultra-high-performance seawater sea-sand concrete. *Adv. Struct. Eng.* **2019**, *22*, 3100–3120. [CrossRef]
43. Huang, B.T.; Wang, Y.-T.; Wu, J.Q.; Yu, J.; Dai, J.G.; Leung, C.K. Effect of fiber content on mechanical performance and cracking characteristics of ultra-high-performance seawater sea-sand concrete (UHP-SSC). *Adv. Struct. Eng.* **2021**, *24*, 1182–1195. [CrossRef]
44. Liao, J.; Yang, K.-Y.; Zeng, J.-J.; Quach, W.-M.; Ye, Y.-Y.; Zhang, L. Compressive behavior of FRP-confined ultra-high performance concrete (UHPC) in circular columns. *Eng. Struct.* **2021**, *249*, 113246. [CrossRef]
45. Huang, B.T.; Yu, J.; Wu, J.Q.; Dai, J.G.; Leung CK, Y. Mechanical performance of seawater sea-sand engineered cementitious composites. *Compos. Commun.* **2020**, *20*, 100353. [CrossRef]
46. Huang, B.T.; Wu, J.Q.; Yu, J.; Dai, J.G.; Leung, C.K. High-strength seawater sea-sand engineered cementitious composites (SS-ECC): Mechanical performance and probabilistic modeling. *Cem. Concr. Compos.* **2020**, *114*, 103740. [CrossRef]
47. Huang, B.T.; Wu, J.Q.; Yu, J.; Dai, J.G.; Leung, C.K.; Li, V.C. Seawater sea-sand engineered/strain-hardening cementitious composites (ECC/SHCC): Assessment and modeling of crack characteristics. *Cem. Concr. Res.* **2021**, *140*, 106292. [CrossRef]
48. Xu, L.Y.; Huang, B.T.; Li, V.C.; Dai, J.G. High-strength high-ductility Engineered/Strain-Hardening Cementitious Composites (ECC/SHCC) incorporating geopolymer fine aggregates. *Cem. Concr. Compos.* **2021**, *125*, 104296. [CrossRef]
49. Huang, B.T. Fatigue Performance of Strain-Hardening Fiber-Reinforced Cementitious Composite and Its Functionally-Graded Structures. Ph.D. Thesis, Zhejiang University, Hangzhou, China, 2018.